3A.1

OBSERVATIONS AND MODELING OF STRUCTURAL-OPTICAL PROPERTIES IN FIRST-YEAR SEA ICE

Bonnie Light*
University of Washington, Seattle, Washington

1. INTRODUCTION

An understanding of radiative transfer in sea ice is critical to understanding the heat and mass balance of the Arctic. Radiative transfer affects such processes as surface melting, ice-albedo feedback, solar heating of the upper ocean, and internal heat storage within the ice. Large temporal changes in the physical state of the ice cover cause large changes in its radiative properties, particularly during the summer. As the surface warms, melts, and forms ponds, there is a substantial decrease in its albedo. To better model changes in the physical state of the ice and its ability to backscatter light, we need a more complete understanding of its fundamental optical properties.

Sea ice is a lattice of nearly pure ice with embedded inclusions of brine, vapor, precipitated salts, and occasional particulate material. The optical properties are determined not only by the bulk volumes of these constituents and their dielectric properties, but also by the inclusion distributions. While numerous studies have been done on the structural properties of sea ice (e.g. Weeks and Ackley, 1981; Perovich and Gow, 1991, 1996), and its optical properties (see Perovich, 1996), relationships between the two have not yet been firmly established.

Because changes in temperature cause the relative amounts of ice, brine, vapor, and precipitated salt to adjust according to freezing equilibrium relationships (Cox and Weeks, 1983), we expect the optical properties of ice to also depend on temperature. The focus of this work is to improve our understanding of how temperature-dependent changes in microstructure govern the inherent optical properties of first-year sea ice.

2. APPROACH

Since little is known about how inclusions of brine, vapor, and precipitated salt are distributed within the ice, and how these distributions relate to the optical properties of the ice, a study was designed to simultaneously collect detailed information on the microstructure and optical properties of interior first-year sea ice over a wide range of temperatures.

As it was not feasible to make these measurements in the field, samples of natural ice were monitored in a temperature-controlled laboratory coldroom. A high-resolution imaging system (Panasonic CCD WV-540 black and white camera and Leica Monozoom Lens)

_____

*Corresponding author address: Bonnie Light, Department of Atmospheric Sciences, Box 351640, University of Washington, Seattle, WA 98195; email: bonnie@atmos.washington.edu

was used to monitor changes in ice microstructure, while a photometric system (Spectron Engineering visible photospectrometer) was used to monitor changes in apparent optical properties. Vertical thin sections (~2.0 mm thick) were used for the structural observations and 5.0 cm-thick core sections were used for the optical observations. The samples were taken from adjacent locations (depth ~80 cm) on the same core, and were kept at approximately identical temperatures in the laboratory. The observations from the two experiments were used to develop and test a structural-optical model where inherent optical properties are predicted directly from information about the ice temperature, density, salinity, and type (see Light, 2000). The samples were first characterized at −15 °C, after which cooling and warming experiments were performed.

3. STRUCTURAL RESULTS

3.1 Observations at −15 °C

Imagery of the microstructure at −15 °C (e.g., Fig. 1) revealed numerous brine (arrow A) and vapor (arrow B) inclusions in the ice. Brine inclusion shapes ranged from approximately spherical to highly elongated, but all were oriented with their long dimension approximately vertical in the ice. More than 1600 brine inclusions were counted, with long dimension (l) ranging from 10 μm to 8.0 mm. The following power law describes ($r^2 = 0.92$) their observed size distribution $N_b(l)$ (Fig. 2):

$$N_b(l) = 0.28\, l^{-1.96} \qquad (1)$$
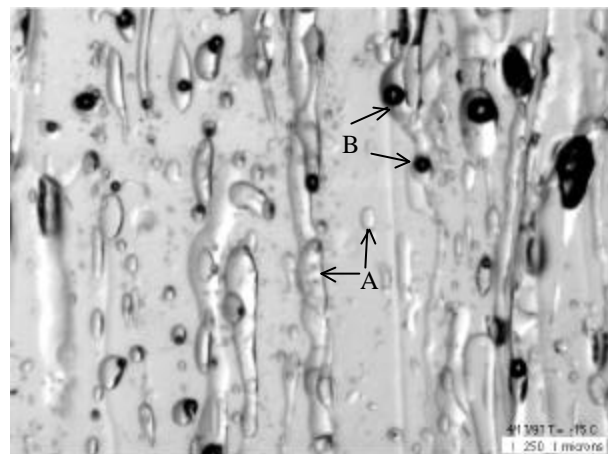
Figure 1. Microphotograph from a structural sample of first-year ice approximately 2 mm thick. The temperature was −15 °C and the sample salinity approximately 3 ppt.

The smallest inclusions observed were an order of magnitude smaller than previously reported (Perovich and Gow, 1996). The integrated number density for these inclusions was approximately 24 per mm^3, also an order of magnitude higher than previously reported (Perovich and Gow, 1996). Length-to-diameter aspect ratios ranged between 1 and 70.
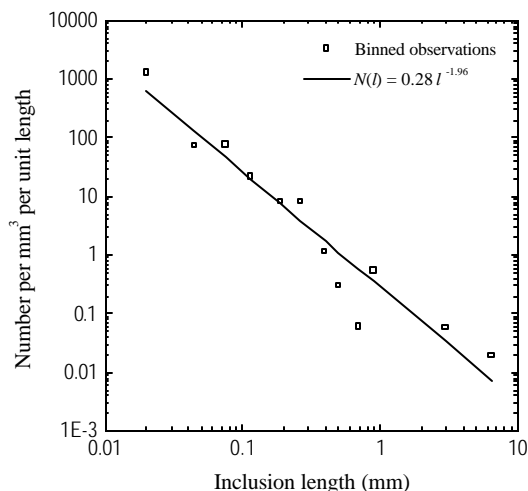
Figure 2. Observed size distribution for brine inclusions in interior first-year sea ice at –15 °C with salinity 3 ppt.

A vapor bubble size distribution was also estimated using the imagery. All bubbles were observed to be within brine inclusions. As with brine inclusions, a power law was used to describe ($r^2 = 0.94$) the observed bubble size distribution as a function of bubble radius (r_v):

$$N(r_v) = 0.06 \, r_v^{-1.5}. \qquad (2)$$

Bubbles were found to be an order of magnitude smaller and 40 times more numerous than previously reported for bubbles in young sea ice (Grenfell, 1983).

As sea ice cools, included brine becomes more concentrated and gradually saturates with respect to certain salts. The two most abundant salts are mirabilite ($Na_2SO_4 \cdot 10H_2O$) and hydrohalite ($NaCl \cdot 10H_2O$). Mirabilite begins to precipitate at –8.2 °C and hydrohalite at –22.9 °C. Mirabilite crystals were frequently visible within large brine inclusions at –15 °C. It is expected that mirabilite was present in all brine inclusions, but smaller inclusions probably contained crystals smaller than 10 μm, and could not be resolved in this study.

3.2 Cooling experiments

Upon cooling, brine inclusions and vapor bubbles were observed to shrink and the amount of visible mirabilite increased. The observed changes in volume were consistent with changes predicted by freezing equilibrium. At temperatures below –22.9 °C, large brine tubes were occasionally observed to become opaque, presumably filled with an ice-hydrohalite slush. Despite this appearance, precipitated hydrohalite was not

observed in a majority of the inclusions. In general, the overall structure was observed to change little as the ice was cooled beyond –22.9 °C.

3.3 Warming experiments

As the ice was warmed to –5 °C, existing brine and vapor inclusions were observed to increase in size and precipitated salt crystals were observed to dissolve. As with cooling, the observed changes were consistent with freezing equilibrium. Bubble nucleation was expected in inclusions that previously had no bubble as cold ice warms and lower density ice melts into higher density liquid water along inclusion walls. Surprisingly, vapor bubble nucleation was generally not observed.

At temperatures above –5 °C, existing brine and vapor inclusions increased dramatically in size. Near the melting temperature, brine inclusions became very large and frequently merged with neighboring inclusions.

4. SCATTERING COEFFICIENT MODEL

The structural data was used to estimate scattering coefficients for brine inclusions, vapor bubbles, and salt crystals. This was done using the formulation of Grenfell (1983, 1991) and an equivalent spherical representation for treating non-spherical inclusions (Grenfell and Warren, 1999). The scattering coefficient (s) for each constituent was computed using the following equation:

$$s = \int_{r_{min}}^{r_{max}} Q(r_{es}) p r_{es}^2 N_{es}(r_{es}) dr_{es}, \qquad (3)$$

where r_{min} and r_{max} are the lower and upper limits of the size distribution, r_{es} is the equivalent spherical radius, and N_{es} is the equivalent spherical number density. $Q[r_{es}]$ is the scattering efficiency, and is taken to be 2 for the inclusions in this study since r_{es} is assumed to much larger than visible light wavelengths.

Equation (3) was applied to brine inclusions, vapor bubbles, and precipitated salts at –15 °C. Values of s for temperatures between –35 and –2 °C were then computed using the structural data at these temperatures, along with information about the bulk volumes according to freezing equilibrium (Fig. 3).

Because sufficient information about the size distributions of the precipitated salts was lacking, a simple formulation presented by Light (1995) was used for a hydrohalite crystal size of 17 μm. Figure 3 shows large changes in the total scattering coefficient when the temperature is low (T < -22.9 °C) owing to the substantial scattering predicted to result from the precipitation of hydrohalite. At higher temperatures (T > -5 °C), large changes in scattering should result from the large increases in brine volume. However, at intermediate temperatures, the calculation predicts that the total scattering coefficient is relatively constant, resulting from a balance between increased scattering due to enlarging brine inclusions and decreased scattering due to dissolving mirabilite crystals. These three temperature regimes can be described as the hydrohalite, mirabilite, and warm-ice regimes.
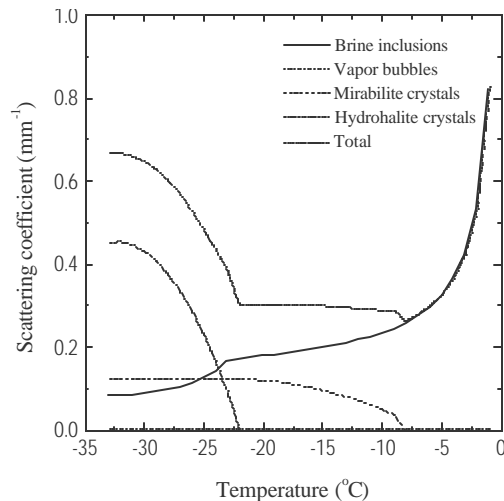
Figure 3. Temperature-dependent scattering coefficients (eq. 3) for brine pockets, tubes, vapor bubbles, and precipitated salt crystals for a 3 ppt salinity sample.

5. OPTICAL RESULTS

Samples used for monitoring apparent optical properties were cylindrical with diameter 10 cm and height 5 cm. In the darkened coldroom, the top surface of the sample was illuminated with incandescent collimated light. A fiber optic probe was used to sample light backscattered and transmitted from the sample at 30 and 70 degrees from zenith and nadir. The probe was coupled to a spectrophotometer and spectral scans were recorded. Radiances were normalized to a reference value, as no attempt was made to monitor absolute radiometric quantities.

The backscattered and transmitted radiances were compared with apparent optical properties predicted with a radiative transfer model specifically designed to solve the radiative transfer equation for a cylindrical domain (Light et al., in preparation). This comparison, along with a simple assumption about the magnitude of the scattering asymmetry parameter for sea ice (g=0.978) was used to infer temperature-dependent scattering coefficients from the optical observations.

Data from a 4.7 ppt salinity optical sample are shown in Fig. 4. In contrast to the structural observations, the optical observations showed large changes in scattering at low temperatures, and surprisingly small changes at higher temperatures.

6. STRUCTURAL-OPTICAL RESULTS

The scattering coefficients inferred from the optical observations were compared with the scattering coefficients calculated using eq. 3 (Fig. 4). The calculated values increased by ~30% when the model was adjusted to account for the additional 1.7 ppt salinity of the optical sample.

In the hydrohalite regime, scattering in the ice is large and is dominated by the presence of hydrohalite crystals. At these temperatures, the scattering is only loosely tied to the ice microstructure because the salts precipitate as a result of brine chemistry and we believe their precipitation patterns are likely not dependent on the size distribution of the brine inclusions. Currently, the model overestimates the scattering by hydrohalite and clearly more work needs to be done to understand the precipitation patterns of these crystals.

In the mirabilite regime, scattering by mirabilite crystals and brine inclusions offset one another. Upon warming, mirabilite crystals dissolve, thus reducing their scattering cross-section, while brine inclusions increase in size, increasing their contribution to the total scattering. While the changes in scattering due to the crystals are only loosely tied to the microstructure, the changes in scattering due to the brine inclusions are tightly tied to the microstructure. Additional observations suggest this balance may be fundamental to sea ice (Light, 1995).

In the warm regime, however, the optical properties did not respond to changes in temperature, while the structural properties indicated that there should be large increases in scattering due to large increases in brine volume. This large discrepancy necessitates inclusion of additional model physics.
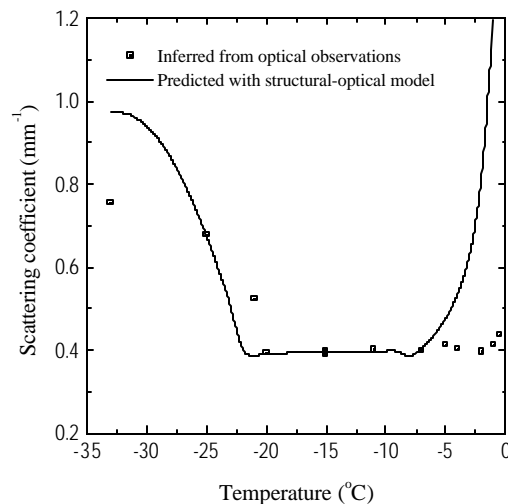
Figure 4. Comparison of scattering coefficient inferred from optical measurements and calculated with structural-optical model for an ice salinity of 4.7 ppt.

7. WARM ICE REGIME

Because the optical observations indicated very little change in the total scattering at warm temperatures, it became necessary to examine the physical properties of sea ice near its melting temperature in more detail.

The effect of brine inclusion merging was first considered. We hypothesized that the total scattering incurred by brine inclusions could be reduced if there were a significant decrease in population surface area that occurred when inclusions merged. Several case studies were selected from the high-temperature imagery and the magnitude of this effect was found to be small.

To explain the bulk of the discrepancy, it was necessary to consider the dramatic change in dielectric

properties of the brine as the ice warms. Because increasing the ice temperature increases the brine volume, the brine dilutes as it warms. This reduction in brine salinity causes the real refractive index of the brine to become closer to that of ice (Maykut and Light, 1995), thus increasing the forward scattering of brine inclusions. Mie theory was used to estimate the change in g as the ice warmed. A similarity parameter was used to assess the impact of this on the total scattering coefficient, and the improved model explained the scattering inferred from the optical observations(Fig. 5).
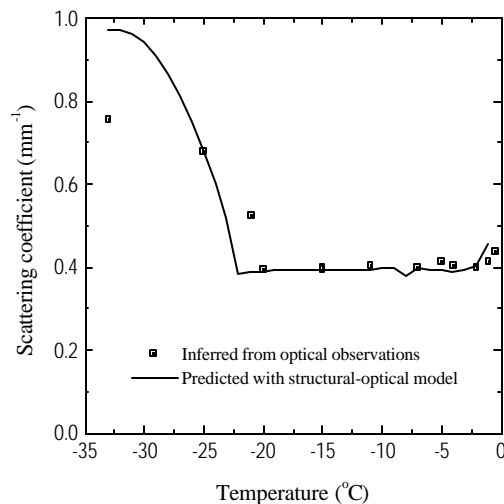
Figure 5. Same as Fig. 4 with increased forward scattering accounted for in the warm-ice regime.

8. CONCLUSIONS

At low temperatures, the optical properties showed large changes in scattering as a function of temperature. These changes are attributed to the precipitation of hydrohalite crystals. Because there is no evidence that the precipitation of these crystals depends on the distribution of brine inclusions in the ice, it is likely that the scattering in this regime is only loosely tied to the ice microstructure. Owing to the fact that the total mass of precipitated hydrohalite will be proportional to the ice salinity, we also expect the scattering in this regime to be tightly tied to the ice salinity.

At more moderate temperatures the optical properties remain approximately constant. We believe this is due to the balance between increased scattering due to enlarging brine inclusions and decreased scattering due to dissolving mirabilite crystals. Additional laboratory data on the optical properties of high-salinity laboratory-grown ice suggest that this balance may exist independent of ice salinity (Light, 1995). Like the hydrohalite, the scattering due to the mirabilite is only loosely tied to the ice structure. Mirabilite crystals precipitate in inclusions, regardless of the inclusion size or shape. In contrast, the scattering due to the brine is tightly tied to the actual brine inclusion distribution.

At higher temperatures, the optical properties of the ice are approximately constant with temperature. There are no appreciable precipitated salts at these temperatures, and the structural observations indicate that changes in the microstructure are substantial. By accounting for the increasingly forward-peaked phase function that results from the decreasing refractive index of the brine, the structural-optical model correctly predicts the reduced scattering as the ice approaches melt. Because of this, the optical properties of the ice at higher temperatures are again only loosely tied to the structure of the ice and become increasingly dependent on the dielectric properties of the brine.

This study suggests that it is possible to employ simple parameterizations for the relationships between the physical properties of the ice and its optical properties. Clearly, the details of the microstructure play a role in determining how the ice interacts with shortwave radiation, but at high temperatures, the optical properties become less sensitive to small variations in the structure.

9. REFERENCES

Cox, G. F. N., and W. F. Weeks, Equations for determining the gas and brine volumes in sea-ice samples, *J. Glaciol., 29*, 306-316, 1983.

Grenfell, T. C., A theoretical model of the optical properties of sea ice in the visible and near infrared, *J. Geophys. Res., 88*, 9723-9735, 1983.

Grenfell, T. C., A Radiative transfer model for sea ice with vertical structure variations, *J. Geophys. Res., 96*, 16991-17001, 1991.

Grenfell, T. C., and S. G. Warren, Representation of a nonspherical ice particle by a collection of independent spheres for scattering and absorption of radiation, *J. Geophys. Res., 104*, 31697-31709, 1999.

Light, B., A structural-optical model of cold sea ice, M.S. thesis, Univ. Wash., Seattle, 1995.

Light, B., Structural-optical relationships in first-year sea ice, Ph.D. dissertation, Univ. Wash., Seattle, 2000.

Maykut, G. A., and B. Light, Refractive-index measurements in freezing sea-ice and sodium chloride brines, *Appl. Opt. 34*, 950-961, 1995.

Perovich, D. K., The optical properties of sea ice USA Cold Regions Research and Engineering Laboratory, Monograph 96-1, Hanover, NH, 1996.

Perovich, D. K., and A. J. Gow, A statistical description of the microstructure of young sea ice, *J. Geophys. Res., 96*, 16943-16953, 1991.

Perovich, D. K., and A. J. Gow, A quantitative description of sea ice inclusions, *J. Geophys. Res., 101*, 18327-18243, 1996.

Weeks, W. F. and S. F. Ackley, The growth, structure, and properties of sea ice, USA Cold Regions Research and Engineering Laboratory, Monograph 82-1, Hanover, NH, 1981.